Review Article | Neuroimaging and Head & Neck

https://doi.org/10.3348/kjr.2017.18.1.180
pISSN 1229-6929 · eISSN 2005-8330
Korean J Radiol 2017;18(1):180-193

Korean Journal of Radiology
KJR

High-resolution Imaging of Neural Anatomy and Pathology of the Neck

Jeong Hyun Lee, MD, PhD[1], Kai-Lung Cheng, MD[2, 3, 4], Young Jun Choi, MD[1], Jung Hwan Baek, MD, PhD[1]

[1]Department of Radiology, University of Ulsan College of Medicine, Asan Medical Center, Seoul 05505, Korea; [2]Department of Medical Imaging, Chung Shan Medical University Hospital, Taichung 402, Taiwan; [3]School of Medical Imaging and Radiological Sciences, Chung Shan Medical University, Taichung 402, Taiwan; [4]Department of Veterinary Medicine, National Chung Hsing University, Taichung 402, Taiwan

The neck has intricately connected neural structures, including cervical and brachial plexi, the sympathetic system, lower cranial nerves, and their branches. Except for brachial plexus, there has been little research regarding the normal imaging appearance or corresponding pathologies of neural structures in the neck. The development in imaging techniques with better spatial resolution and signal-to-noise ratio has made it possible to see many tiny nerves to predict complications related to image-guided procedures and to better assess treatment response, especially in the management of oncology patients. The purposes of this review is to present imaging-based anatomy of major nerves in the neck and explain their relevant clinical significance according to representative pathologies of regarded nerves in the neck.

Keywords: *Magnetic resonance imaging; Neck; Vagus nerve; Cervical plexus; Brachial plexus; Sympathetic ganglion; Spinal accessory nerve; Anatomy; Pathology; Cervical vertebrae*

INTRODUCTION

The neck has neural structures intricately connected to the skull base, cervicothoracic spine, upper extremities, or functional end organs located in the neck. These neural structures include cervical and brachial plexi, the sympathetic system going into the skull base and the bilateral orbit, lower cranial nerves from IX to XII, and their branches. Although the brachial plexus has been intensely investigated with MRI, there has been little research regarding the normal imaging appearance or the corresponding pathologies of other neural structures using CT or MRI probably due to their complex anatomies and small dimensions. However, the development of imaging techniques with better resolution and signal-to-noise ratio can now enable the visualization of tiny neural structures, consequently making it possible to predict complications related to image-guided minimally invasive procedures such as tumor ablation and core needle biopsy that have gained increased popularity as alternatives to surgery. CT and MRI have also been increasingly used in oncology patients before and after treatment or to assess tumor response after chemoradiation therapy and the use of cytostatic drugs. For those purposes, it is important to know the normal findings and pathologic findings of neural structures on CT or MR for better prediction of patient outcomes and management. Therefore, the purpose of this review was to systematically present imaging-based anatomy and landmarks of major neural structures in the neck. By presenting their normal imaging appearance on CT or MRI, their relevant clinical significance and representative pathologies of the regarded nerves in oncology patients before and after treatment are explained in this study.

Received February 21, 2016; accepted after revision July 10, 2016.
Corresponding author: Jeong Hyun Lee, MD, PhD, Department of Radiology, University of Ulsan College of Medicine, Asan Medical Center, 88 Olympic-ro 43-gil, Songpa-gu, Seoul 05505, Korea.
• Tel: (822) 3010-4355 • Fax: (822) 476-0090
• E-mail: jeonghlee@amc.seoul.kr

Korean Journal of Radiology
KJR

Imaging Anatomy and Pathologies of the Major Nerves in the Neck

Cervical Sympathetic Trunk

Cervical ganglia are composed of three paravertebral ganglia of the sympathetic nervous system. Superior cervical sympathetic ganglion (CSG), the largest one, is located close to the longus capitis muscle at the level of C2/C3 transverse process. Middle CSG, the smallest one, lies close to the inferior thyroid artery at the level of C6/C7 intervertebral disc. Inferior CSG, the intermediate in size, is 80% fused with the first thoracic ganglion to form a star-shaped enlargement called stellate ganglion. It is located lateral to the longus colli muscle at the level of C7/T1 vertebra (Fig. 1A) (1). Cadaveric studies have revealed that all specimens have the superior and inferior CSGs. Only one-third to less than half of specimens have middle CSGs (2). Injury to the CSG can cause ipsilateral blepharoptosis, pupillary miosis, and facial anhidrosis (also known as Horner's syndrome) (3).

A recent study using 3T-MRI has revealed that 73% of superior CSGs can be identified in medial to internal carotid artery (ICA) and lateral to longus capitis muscle at the level of C2 or C3 vertebra (4) with a 3-dimensional size of 0.5–1.3 cm in width, 0.2–0.6 cm in thickness, and 1.5–4.5 cm in length. Other superior CSGs have positional variations (4), including anterior to longus capitis muscle (18%), lateral to ICA (7%), and posterior to ICA (3%) (Fig. 2). The authors of that study have suggested that intraganglionic hypointensity 'on both T2WI and CET1WI' as well as their typical location can be used as imaging clues for differentiating SCSGs from retropharyngeal lymph node metastasis (Fig. 3).

The inferior or stellate ganglion can be easily visualized on CT or MR images (5). It is located at the thoracic inlet adjacent to the neck of the 1st rib, lateral to the longus colli muscle, and posterior to the vertebral artery. It is 1–2.5 cm in length, 1 cm in width, and 0.5 cm in thickness (1, 5). Different from the superior and inferior CSGs, the middle CSG has been found in only 41% of normal patients by sonographic studies, in agreement with previous cadaveric results (1, 2, 6). The mean size of the middle CSG is 0.4 cm in width, 0.2 cm in thickness, and 0.9 cm in length. They are mainly located at the C6/C7 level lateral to the common carotid artery (CCA) on ultrasonography (US) corresponding to the posterior position to CCA on CT or MRI (Fig. 4).

Brachial Plexus

The ventral rami of C5–C8 and T1 constitute the brachial plexus that can be divided into roots, trunks, divisions, cords, and terminal branches (Fig. 1B). The brachial plexus gives rise to the motor and sensory innervation to the upper extremities. The five roots are fused to form the upper (C5 and C6), middle (C7), and inferior (C8 and T1) trunks at the

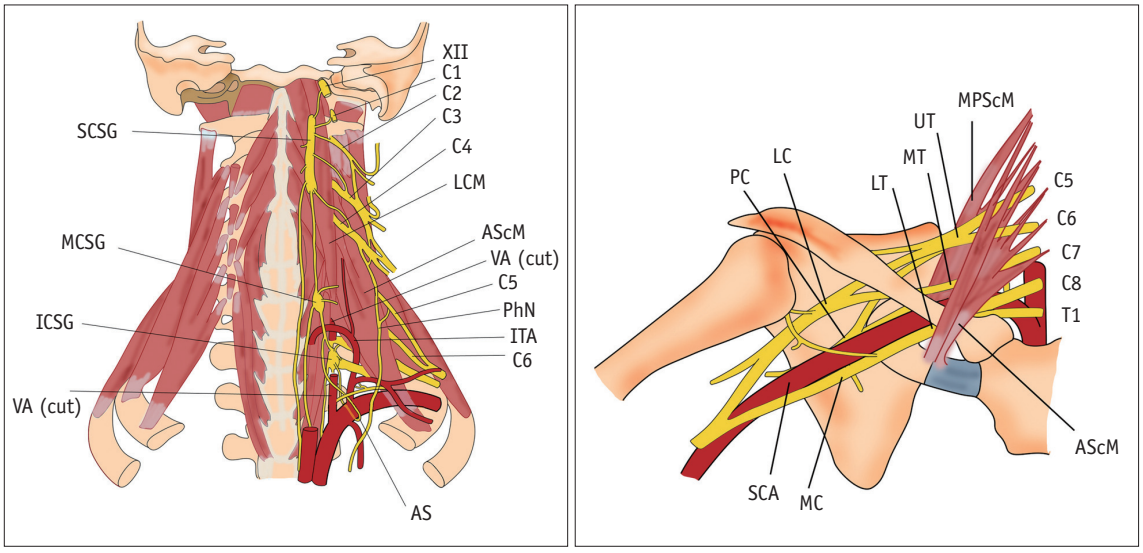

Fig. 1. Diagram of cervical sympathetic trunk (A) and brachial plexus (B). AS = ansa subclavia, AScM = anterior scalene muscle, C1–C8 = 1st to 8th cervical nerves, ICSG = inferior cervical sympathetic ganglion, ITA = inferior thyroid artery, LC = lateral cord, LCM = longus capitis muscle, LT = lower trunk, MC = middle cord, MCSG = middle cervical sympathetic ganglion, MPScM = middle and posterior scalene muscles, MT = middle trunk, PC = posterior cord, PhN = phrenic nerve, SCA = subclavian artery, SCSG = superior cervical sympathetic ganglion, UT = upper trunk, VA = vertebral artery, XII = hypoglossal nerve

level of subclavian artery (SCA) immediately after leaving the interscalene triangle between the anterior and middle scalene muscles. While crossing the clavicle, each trunk is separated into anterior and posterior divisions. The anterior divisions from the upper and middle trunks, the posterior divisions from the upper, middle, and lower trunks, and the anterior divisions of the lower trunk will reunite to form the lateral, posterior, and medial cords around the axillary artery, respectively. After passing the lateral border of the pectoralis minor muscle, these cords are separated into five terminal branches (7).

MRI is the imaging modality of choice to evaluate the anatomy and pathologic conditions of the brachial plexus. Single axial, coronal plane, and sagittal plane are difficult to show the whole course of brachial plexus structures because the image plane is not aligned with the orientation of the brachial plexus. Our standard protocol includes axial T1- and T2-weighted images, coronal T2-weighted images with fat suppression and T1-weighted images, and sagittal T1- and T2-weighted images of the symptomatic side. Oblique planes to the axis of the brachial plexus are not performed because the anatomical relationships are not familiar to radiologists. In addition, the scanograms have to be referred to read the images. Intravenous gadolinium agent is useful in case of tumor. MR myelographic images are reserved for the evaluation of nerve root avulsion or pseudomeningocele. Brachial plexopathy can be caused by trauma, inflammation, neoplastic condition, and extrinsic compression. A neoplastic condition constitutes 60% of non-traumatic brachial plexopathy. It is mostly caused by direct invasion of lymphatic spread from malignant tumors (Fig. 5). Carcinomas of the lung and breast are the most common ones involving the brachial plexus. Lymphoma can involve the brachial plexus in two ways (infiltration of the plexus by affected lymph nodes and by neurolymphoma, i.e., primary lymphoma of the peripheral nerves) (Fig. 6) (8). It

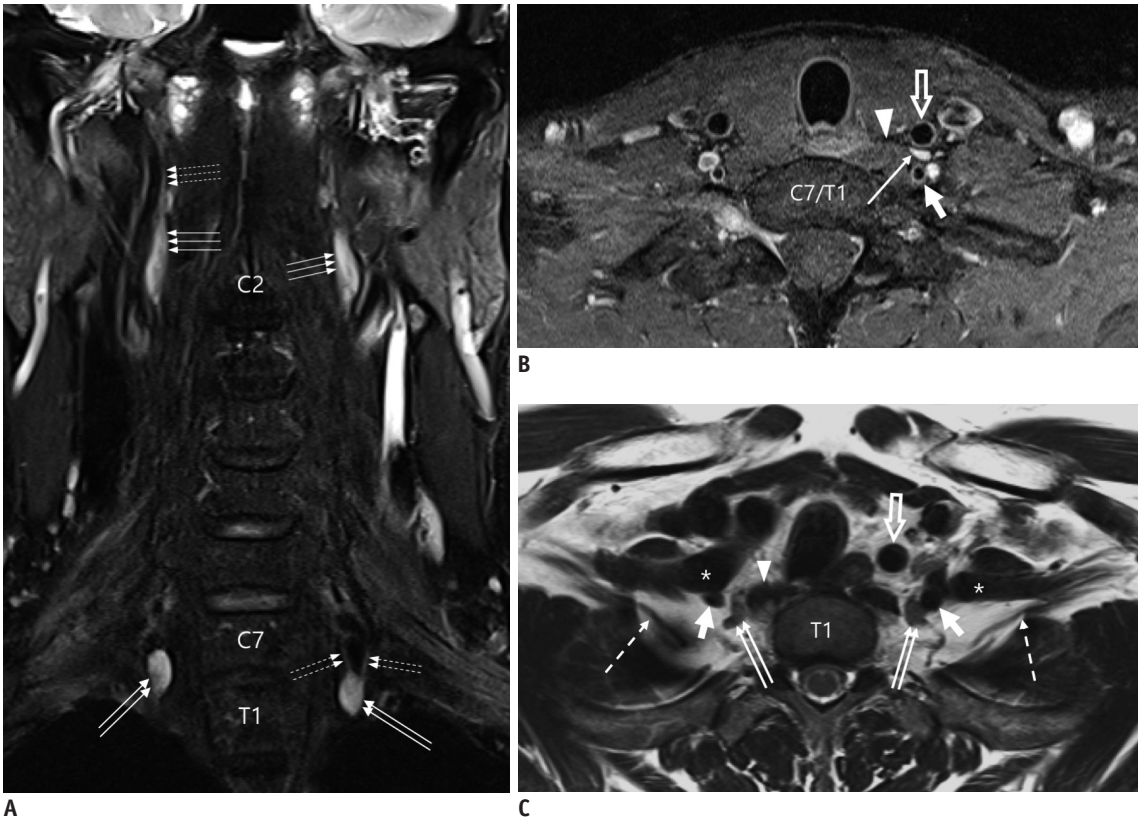

Fig. 2. Normal MRI appearance of cervical sympathetic ganglia (CSGs).
A-C. Coronal fat-suppressed (FS) T2-weighted image (T2WI) **(A)**, axial contrast-enhanced fat-suppressed T1-weighted image **(B)**, and axial T2WI **(C)** demonstrating typical locations and signal characteristics of superior (triple arrows on **A**), middle (single arrow on **B**), and inferior (double arrows on **A** and **C**) CSGs. Coronal FS T2WI **(A)** clearly shows that connecting nerve branches with superior CSG (dotted triple arrows) and inferior CSG (dotted double arrows). Note that middle CSG is located posterior to common carotid artery (empty arrow on **B**), anterior to vertebral artery (VA, short arrow on **B**), and lateral to longus colli muscle (arrowhead on **B**). Inferior CSG on either side is present as stellate ganglion lateral to longus colli muscle (arrowhead on **C**) and posteromedial to origin of VA (short arrows on **C**). Asterisk = subclavian artery, C2 = 2nd vertebra, C7 = 7th vertebra, dotted arrow = T1 nerve root, T1 = 1st thoracic vertebra

Korean Journal of Radiology
KJR

is often difficult to differentiate between recurrent tumor and radiation-induced plexopathy in patients with history of cancer and clinical evidence of plexopathy following radiation therapy. Typical radiation-induced plexopathy is usually low on T1- and low or high on T2-weighted images showing diffuse thickening of the plexus with various degrees of enhancement of the intravenous contrast agent (Fig. 7). Tumors have various signal intensities according to primary tumors. They are usually enhanced by a contrast agent, showing irregular or nodular thickening of the plexus or accompanied by a focal or infiltrative mass (Fig. 8) (9, 10).

Cervical Plexus

The ventral rami of the first four cervical spinal nerves constitute the cervical plexus. They are located in front of the C1 to C4 vertebra, deep and posterior to the sternocleidomastoid muscle (SCM), anterior to the middle scalene muscle, and posterolateral to the longus capitis muscle (Fig. 9). The cervical plexus has cutaneous and muscular branches. Cutaneous branches innervate the skin surrounding the auricle (greater auricular but lesser occipital nerves), neck, and clavicle (transverse cervical and supraclavicular nerves). Muscular branches innervate the infrahyoid muscles (except for the thyrohyoid muscle) and the diaphragm (phrenic nerve) (7). Axial T1-, T2-, and contrast-enhanced T1-weighted images of thin slices (< 3-mm in thickness/no gap) should be used to find their locations due to the small diameter of the branches from the cervical plexus and accompanying venules or arterioles.

The greater auricular nerve is the largest ascending cutaneous branch of the cervical plexus. Arising from the ventral rami of C2 and C3, it goes to the posterior edge of the SCM. After wrapping around the edge of the SCM, it ascends on the outer surface of the muscle beneath the platysma after perforating the deep cervical fascia (7). After

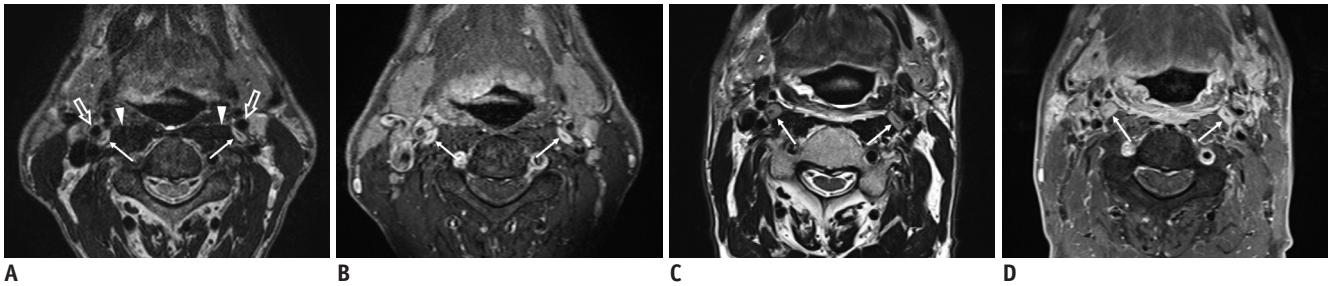

Fig. 3. 60-year-old male with squamous cell carcinoma of right pyriform sinus (T3N1M0) after definitive concurrent chemoradiation therapy.
Pretreatment **(A, B)** and post treatment **(C, D)** axial T2-weighted images (T2WIs) and contrast-enhanced fat-suppressed T1-weighted images (CE FS T1WIs) demonstrate homogeneously enhanced superior cervical sympathetic ganglia (CSG, thin arrows on **A-D**) on either side lateral to longus capitis muscle (arrowheads on **A**) and posterior to internal carotid artery (empty arrows on **A**). Note that there is typical intraganglionic hypointensity at center of superior CSGs both on T2WI and CE FS T1WI. Superior CSGs become enlarged in anterior to posterior dimensions along with diffuse radiation-induced change in retropharyngeal space, pharyngeal wall, and bilateral cervical level II.

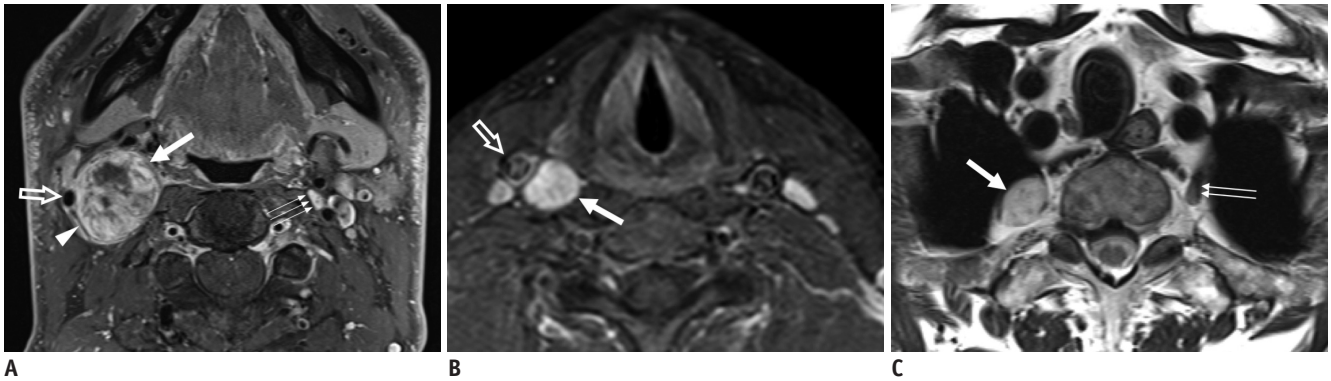

Fig. 4. Schwannomas arising from cervical sympathetic ganglia (CSGs).
Axial contrast-enhanced fat-suppressed T1-weighted images **(A, B)** and axial T2-weighted image **(C)** showing shwannomas arising from superior (thick arrow on **A**), middle (thick arrow on **B**), and inferior (thick arrow on **C**) CSGs. Masses arising from superior and middle CSGs typically displace internal carotid artery (empty arrow on **A**) or common carotid artery (empty arrow on **B**) to lateral side with internal jugular vein (arrowhead on **A**). Triple and double arrows on **A** and **C** showing normal superior and inferior CSGs, respectively.

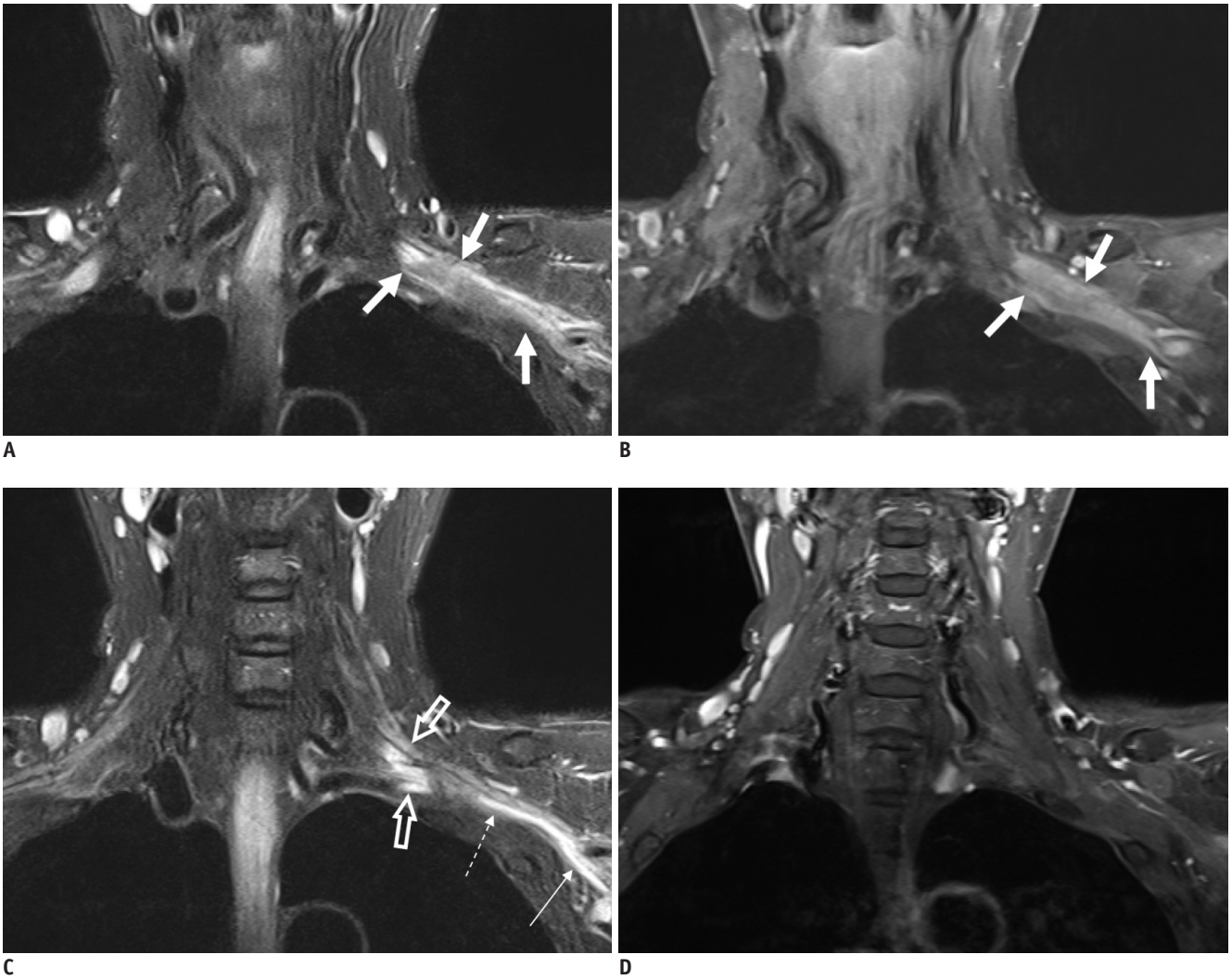

Fig. 5. 58-year-old female with left breast cancer.
Coronal fat-suppressed T2-weighted images (FS T2WIs) **(A)** and contrast-enhanced (CE) FS T1-weighted image (T1WI) **(B)** showing infiltrative and enhanced tumor involving entire trunks of left brachial plexus (arrows). Coronal FS T2WI **(C)** depicts hyperintense change without enhancement of roots (empty arrows), part of lower trunk (dotted arrow), and medial cord (thin arrow) originating from secondary compressive plexopathy, different from infiltrative tumor (thick arrows on **A** and **B**). There is no enhancement at corresponding segments of left brachial plexus on coronal CE FS T1WI **(D)**.

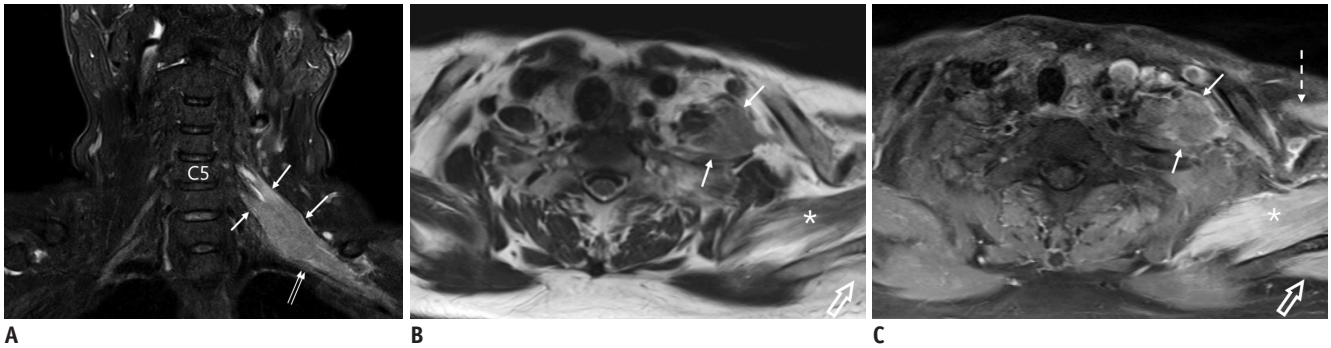

Fig. 6. 66-year-old female with diffuse and large B-cell lymphoma involving brachial plexus.
Coronal fat-suppressed (FS) T2-weighted image (T2WI) **(A)**, axial T2WI **(B)**, and contrast-enhanced (CE) FS T1-weighted image **(C)** demonstrating ill-defined infiltrating mass (arrows on **A-C**) involving left C5 and C6 nerve roots and upper trunk that displaces left middle trunk (double arrows on **A**) inferiorly. Note denervation changes with T2 hyperintensity and homogeneous enhancement of subscapularis (asterisk on **B** and **C**), supraspinatus (empty arrows on **B** and **C**), and pectoralis major (dotted arrow on **C**) muscles.

Korean Journal of Radiology
KJR

passing to the parotid gland, it is divided into two branches innervating the facial skin over the parotid gland ("anterior branch") and the skin over the mastoid process on the back of the auricle ("posterior branch") (Figs. 10, 11).

The supraclavicular nerves arise from a common trunk formed from rami from C3 and C4 nerves. They emerge at the posterior border of the SCM. The trunk descends under the platysma and the deep cervical fascia. It is divided into branches that diverge to pierce the deep fascia above the clavicle slightly. It supplies the skin over the clavicle, upper chest, and part of the shoulder (7).

The phrenic nerve arises chiefly from the C4 ventral ramus. It also receives contributions from the third and fifth cervical nerves. It is formed at the upper part of the lateral border of the anterior scalene muscle. It descends almost vertically across its anterior surface behind the prevertebral fascia (Fig. 12) (7).

The signs and symptoms of cervical plexus damage can vary depending on the severity and the location of the involved nerves. After neck dissection, traumatic neuroma

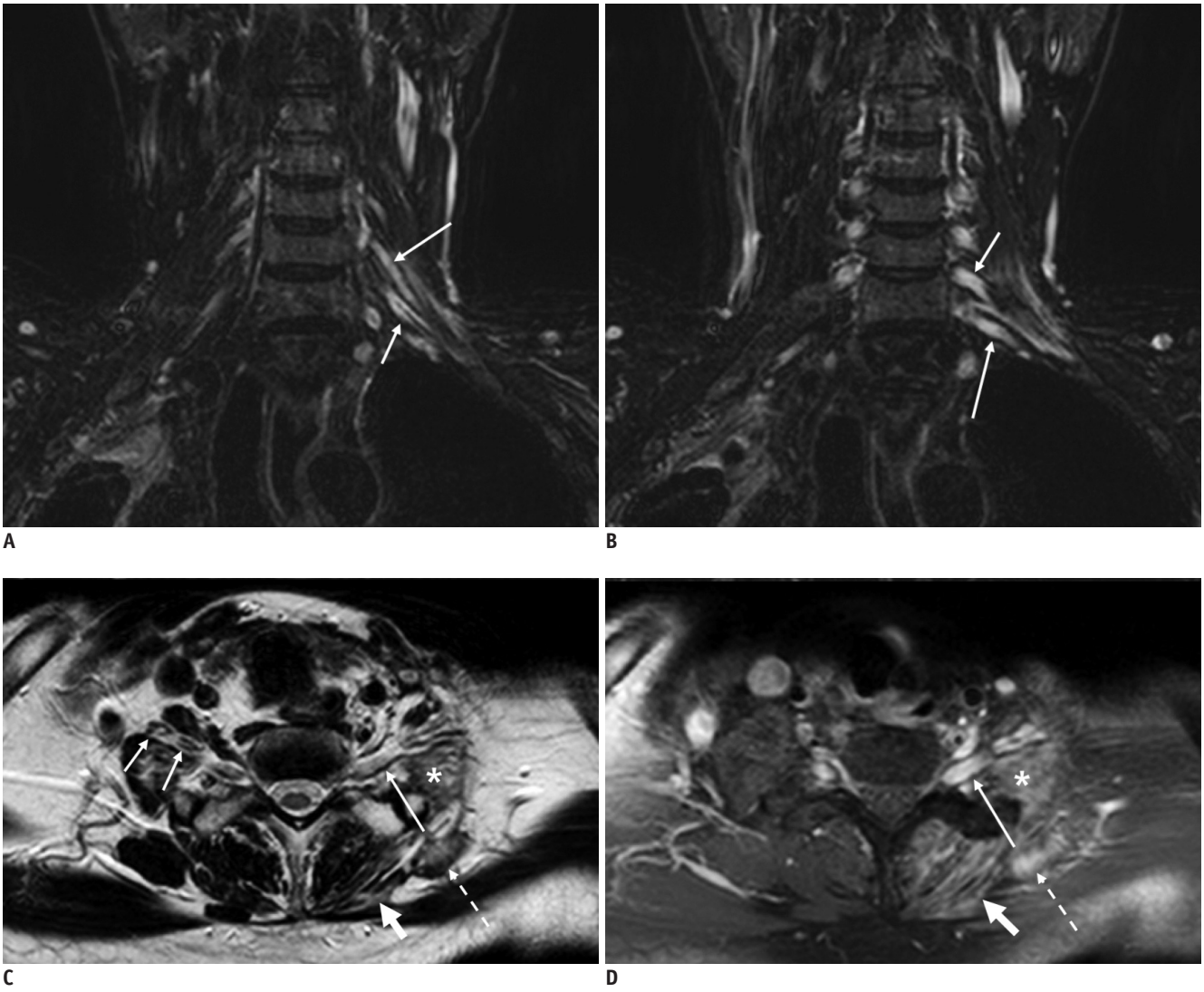

Fig. 7. 56-year-old male with left shoulder weakness after radiation therapy for metastatic lymph nodes in left supraclavicular area due to right lung cancer.
Coronal fat-suppressed (FS) T2-weighted images (T2WIs) **(A, B)** and axial T2WI **(C)** showing marked T2 hyperintensity of left C6 (long arrow on **A**), C7 (short arrows on **A** and **B**), and C8 (long arrow on **B** and **C**) nerve roots caused by radiation-induced brachial plexopathy. There are atrophy, T2 hyperintense change, enhancement of left paravertebral (thick arrow on **C** and **D**), middle and posterior scalene (asterisk on **C** and **D**), and levator scapulae (dotted arrow on **C** and **D**) muscles secondary to plexopathy. Note that C8 nerve roots (long arrow on **D**) are also diffusely enhanced by contrast agent on axial contrast-enhanced FS T1-weighted image **(D)**. Short arrows on **C** denote normal right C6 and C7 nerve roots in interscalene triangle.

usually arises from injury to the peripheral sensory nerves of the cervical plexus as a reparative process at the proximal end of the transected nerve (11, 12). It can be confused with a metastatic lymph node, especially on US. However, identification of the direct continuity of the transected nerve can easily verify a traumatic neuroma, thus avoiding unnecessary biopsy (Fig. 13) (12).

Vagus Nerve

The vagus nerve is the longest cranial nerve. It has the widest distribution in the body. It contains parasympathetic, motor, sensory, and taste fibers. The vagus nerve exits the skull base through the pars vascularis of the jugular foramen. It courses downward within the carotid space, mostly posterolateral to the ICA, and then to the CCA and posteromedial to the internal jugular vein (IJV) (Fig. 14A) (13). The vagus nerve has two marked enlargements, including a smaller superior ganglion located in the middle of the jugular foramen and a larger inferior ganglion located at the level of the transverse process of the C1 vertebra (7, 14). The superior ganglion is spherical and approximately 4 mm in diameter. The inferior or nodose ganglion is elongated and cylindrical in shape with a length of approximately 2.5 cm and a maximum width of 5 mm (Fig. 15) (7). Running down the neck to the level of the thyroid gland, the vagus nerve can change its position relative to CCA. According to US studies, the vagus nerve has anatomical variations in its course (from lateral to anterior

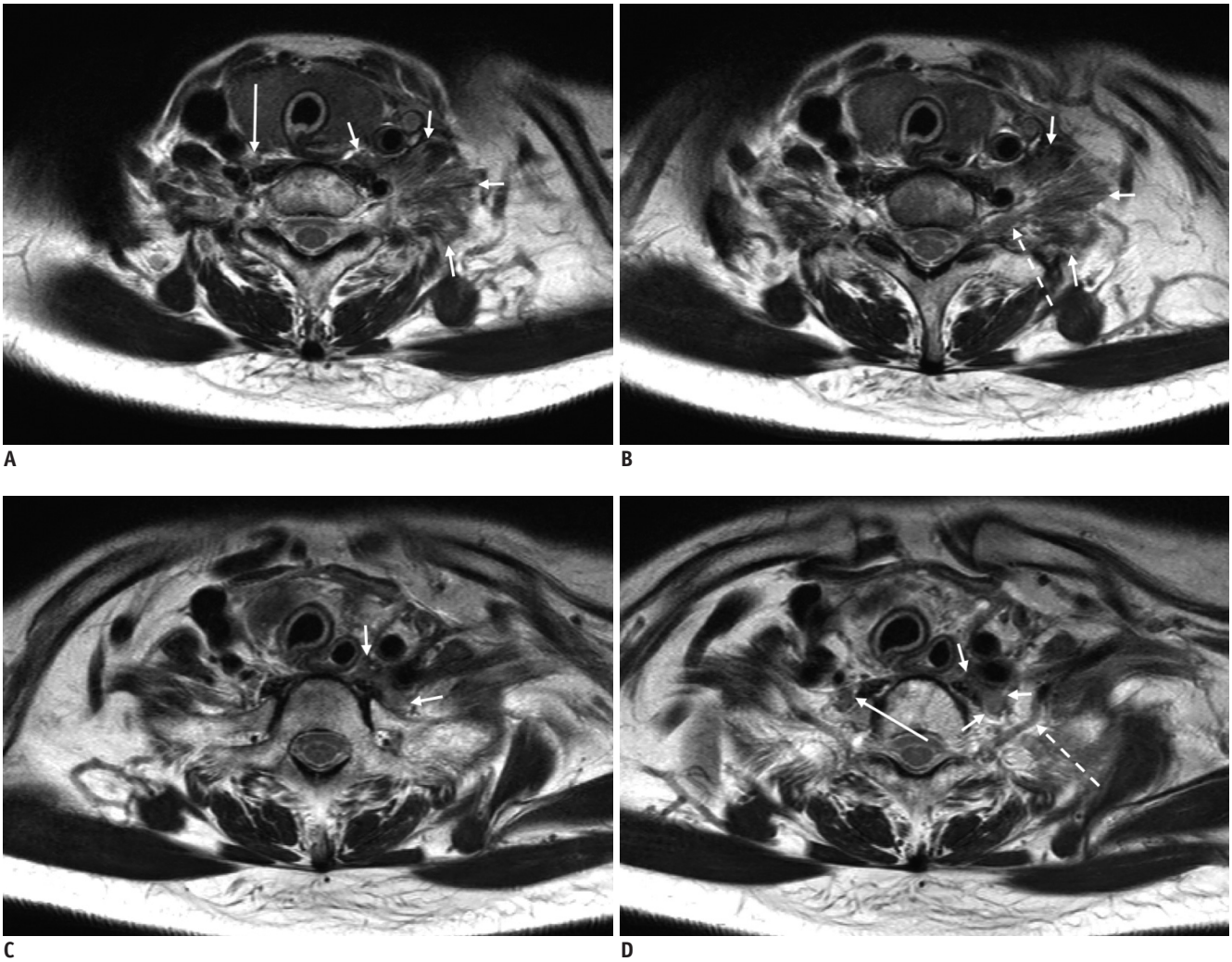

Fig. 8. 55-year-old female with breast cancer and history of lymph node metastasis in left supraclavicular area.
A-D. Axial T2-weighted images for evaluation of recent left Horner's syndrome and brachial plexopathy depicting infiltrating tumor invading longus colli, anterior, middle, and posterior scalene muscles, intervening brachial plexus (short arrows on **A** and **B**), and inferior cervical sympathetic ganglion (CSG, short arrows on **C** and **D**) on left side. Note normal middle CSG (long arrow on **A**) and inferior CSG (long arrow on **D**) on right side. Dotted arrows on **B** and **D** denote C8 and T1 nerve roots, respectively.

Korean Journal of Radiology
KJR

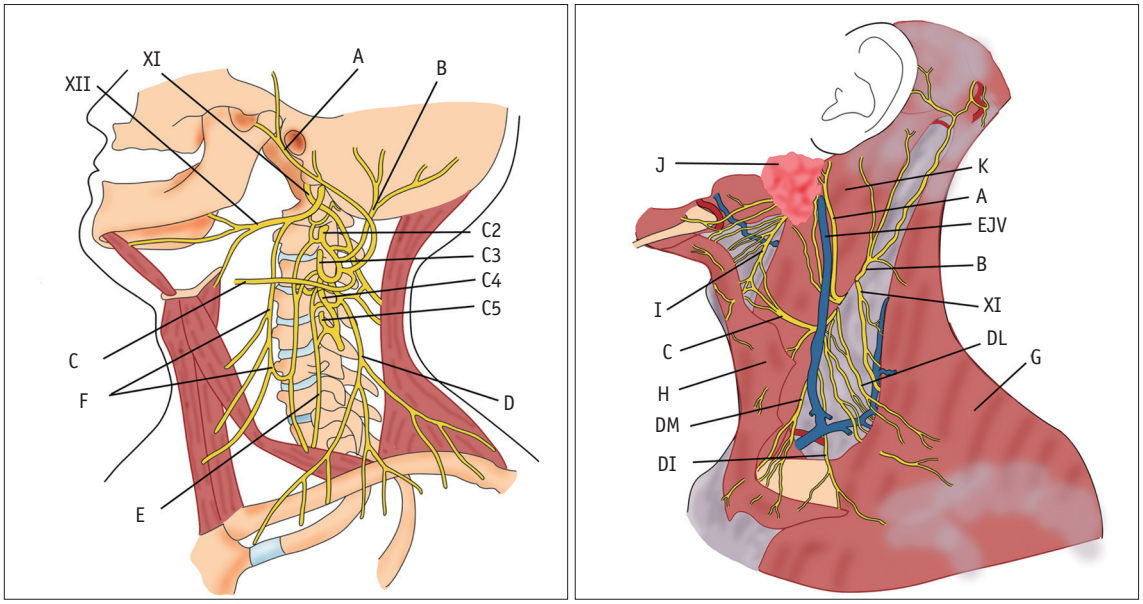

Fig. 9. Diagram of cervical plexus and its branches. A = greater auricular nerve, B = lesser occipital nerve, C = transverse cervical nerve, C2–C5 = 2nd to 5th cervical nerves, D = supraclavicular nerve, DI = intermediate branch, DL = lateral branch, DM = medial branch, E = phrenic nerve, EJV = external jugular vein, F = ansa cervicalis, G = trapezius muscle, H = platysma, I = cervical branch of facial nerve, J = parotid gland, K = SCM muscle, XI = spinal accessory nerve, XII = hypoglossal nerve

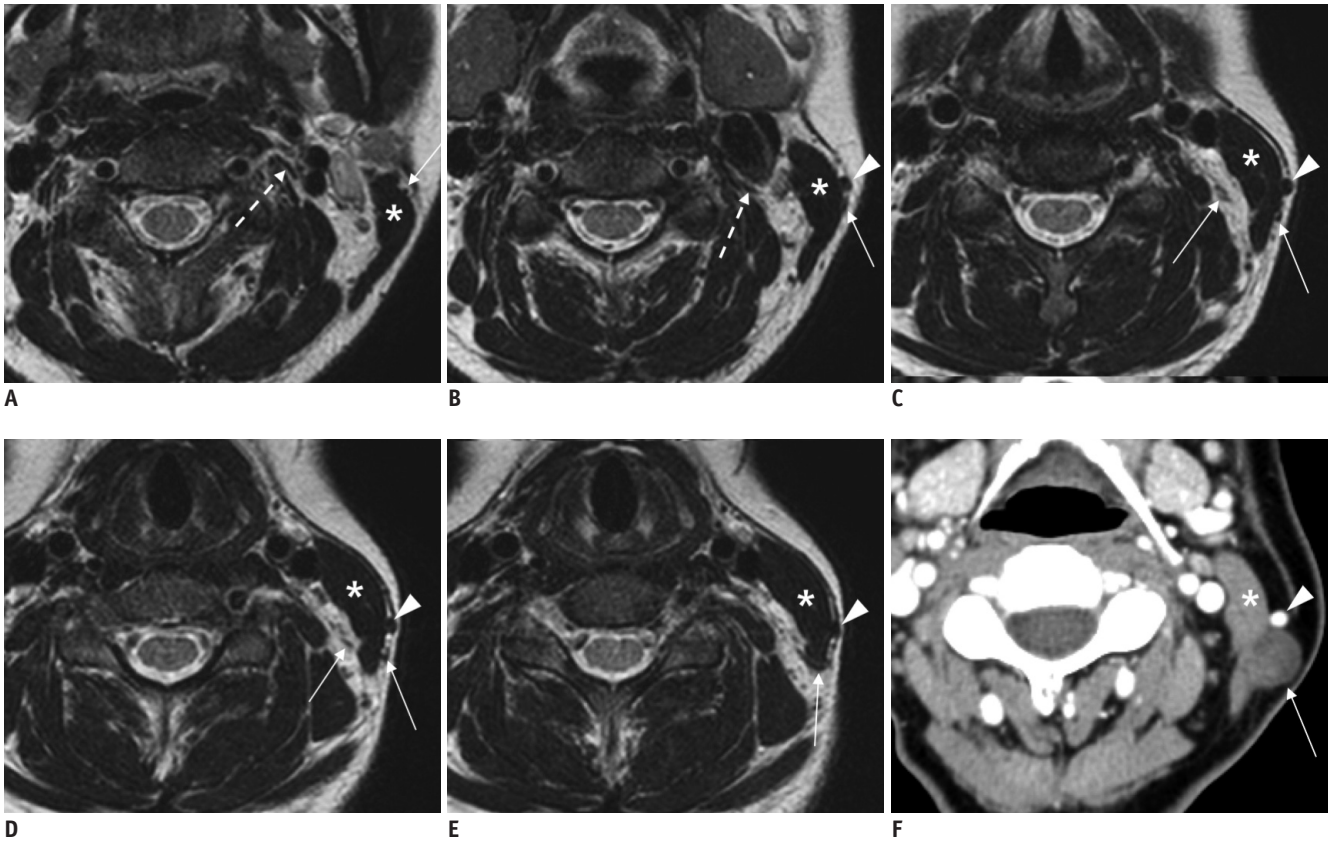

Fig. 10. Imaging appearance of normagreater auricular nerve and its pathology.
A-E. Axial T2-weighted images depicting greater auricular nerve (long arrows) branching off from cervical plexus (dotted arrow on **A** and **B**), running posterolaterally in posterior cervical triangle, and wrapping around edge of sternocleidomastoid muscle (SCM, asterisk) to proceed to parotid gland. Note external jugular vein (EJV, arrowheads) running just anterior to greater auricular nerve on surface of SCM. **F.** Axial CT image showing typical case of schwannoma (arrow) arising from greater auricular nerve on outer surface of SCM (asterisk) posterior to EJV (arrowhead).

in 4.3–21.1% of cases and from lateral to medial in 1.2–1.6% of cases) (13, 15). In one study, there was even posterior variation of vagus nerve in 0.3% of the patients (Fig. 16) (13).

The branches of the vagus in the neck are meningeal, auricular, pharyngeal, carotid body, superior, and recurrent

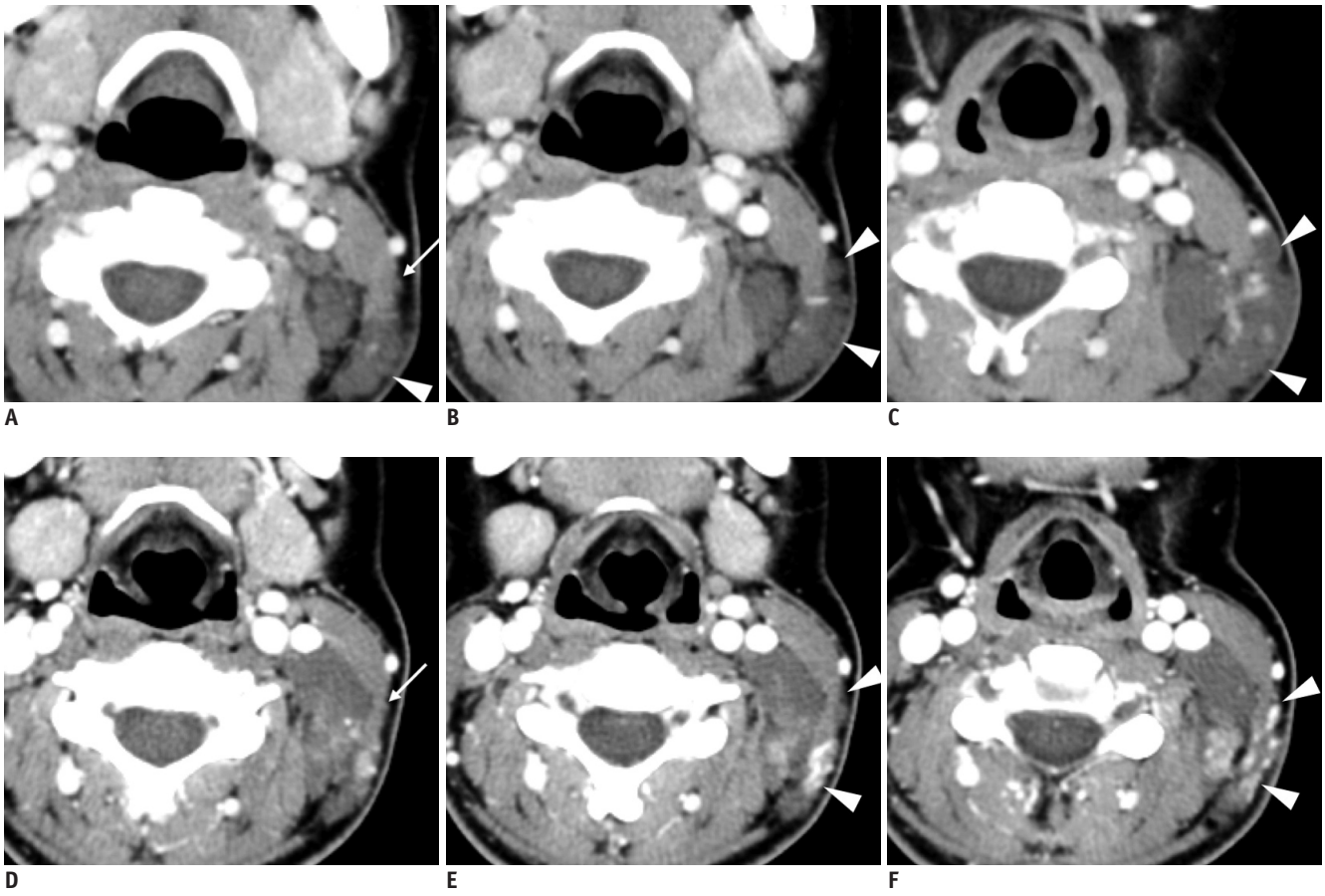

Fig. 11. 24-year-old female with venolymphatic malformation in left posterior cervical triangle treated with radiofrequency ablation.
Pre-treatment axial CT images **(A-C)** showing that part of non-enhancing lobulating mass (arrowheads on **A-C**) is incorporating greater auricular nerve (arrow on **A**). Patient had decreased sensation of left auricle and mastoid area following her treatment. Post-treatment axial contrast-enhanced CT images **(D-F)** showing decreased size with post-treatment enhancement of lesion at edge and posterior surface of sternocleidomastoid muscle (arrowheads on **E** and **F**). Note greater auricular nerve (arrow on **D**) at same location on **A**.

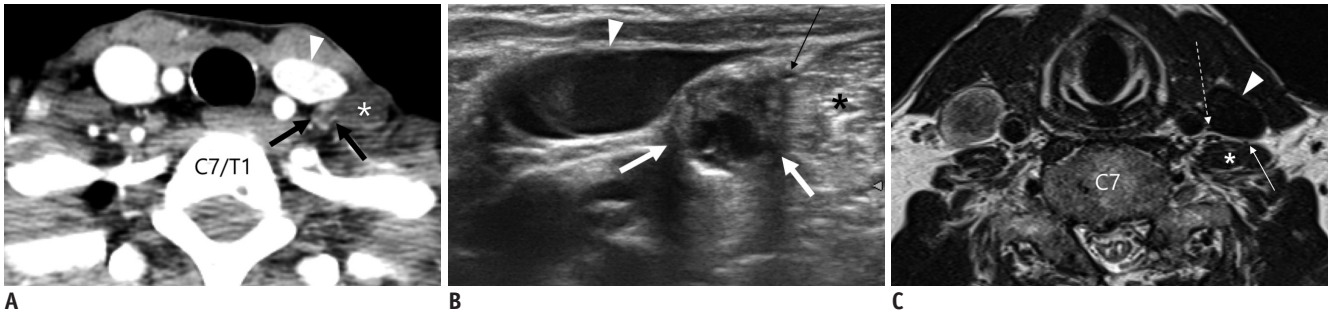

Fig. 12. 56-year-old female with metastatic lymph node in left level IV after total thyroidectomy and left lateral neck dissection.
A. Axial CT image showing enhancing lymph node with cystic change in left level IV (thick arrows) posterior to internal jugular vein (IJV, arrowhead) and anteromedial to left anterior scalene muscle (asterisk). **B.** Transverse ultrasonography image before radiofrequency ablation of lymph node clearly showing that phrenic nerve (thin arrow) is in close contact with metastatic lymph node (thick arrows) anteromedial to left scalene muscle (asterisk). Arrowhead denotes IJV. **C.** Axial T2-weighted image in another patient demonstrating relationship of phrenic nerve (thin arrow), IJV (arrowhead), anterior scalene muscle (asterisk), and vagus nerve (dotted arrow).

Korean Journal of Radiology
KJR

laryngeal nerves cardiac branches. The vagus nerve enters the thorax after descending posterior to the IJV to cross anterior to the SCA on the right side and between the CCA and SCA (behind the brachiocephalic vein) on the left side.

After arising from the vagus in the neck, the superior laryngeal nerve descends by the side of the pharynx medial to the carotid sheath. It is divided into two branches that are approximately 2–3 cm above the thyroid gland (7). The external branch is accompanied by the superior thyroid artery and its branch while the internal branch is accompanied by

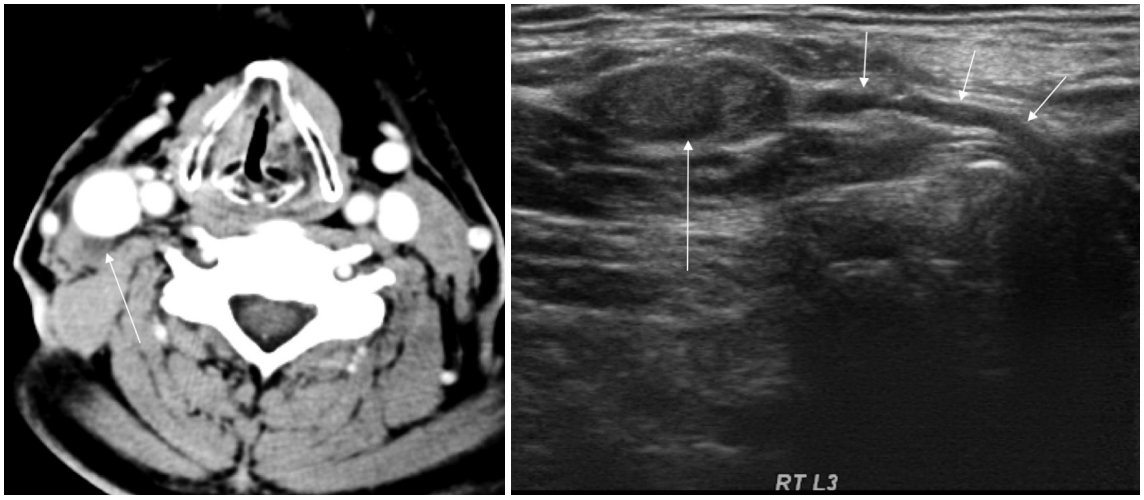

Fig. 13. 66-year-old male after total thyroidectomy and right modified radical neck dissection for thyroid carcinoma.
A. Postoperative axial CT image showing small ill-defined hypoattenuating mass in right level III (arrow). **B.** Ultrasonography image clearly showing C4 spinal nerve (short arrows) continuous from neural foramen to heterogeneous hypoechoic mass (long arrow), thus confirming traumatic neuroma.

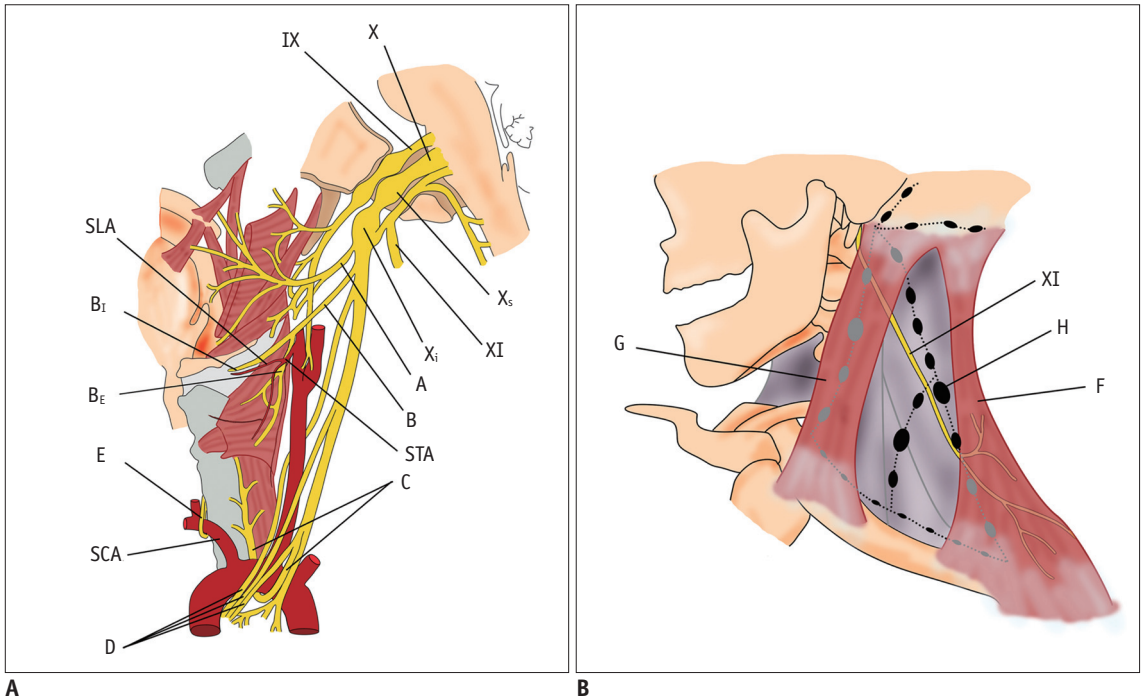

Fig. 14. Distribution of vagus (A) and spinal accessory (B) nerves in neck. A = pharyngeal branch, B = superior laryngeal nerve, B_E = external branch, B_I = internal branch, C = left recurrent laryngeal nerve, D = superior, middle, and inferior cardiac nerves, E = right recurrent laryngeal nerve, F = trapezius muscle, G = sternocleidomastoid muscle, H = lymph node (level V), IX = glossopharyngeal nerve, SCA = right subclavian artery, SLA = superior laryngeal artery, STA = superior thyroid artery, X = vagus nerve, X_s = superior ganglion, X_i = inferior ganglion, XI = spinal accessory nerve

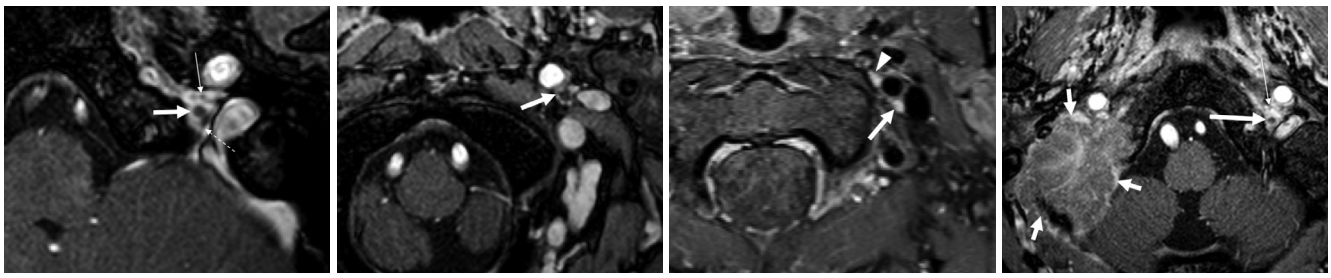

Fig. 15. A, B. Axial three-dimensional contrast-enhanced (CE) T1-weighted turbo field echo (T1-TFE) images (acquisition, 0.6 mm; reconstruction, 1.2 mm) showing relationship of glossopharyngeal (thin arrow on A) and spinal accessory (dotted arrow on A) nerves and superior vagal ganglion (thick arrow on A) at jugular foramen. After exiting jugular foramen, vagus nerve becomes prominent, forming inferior vagal ganglion (thick arrow on **B**). **C.** On CE fat-suppressed (FS) T1-weighted image (turbo spin echo; image acquisition, 3-mm slice thickness with no gap) in different patient, inferior vagal ganglion (thick arrow) is homogeneously enhanced by contrast agent similar to top of superior sympathetic ganglion (arrowhead) located medial to ICA. **D.** Axial CE FS T1-TFE image of patient with metastasis to skull base showing large enhancing mass invading right occipitotemporal bone, including jugular foramen (short arrows) but not containing discernible lower cranial nerves. Note normal, superior vagal ganglion (long arrow), and glossopharyngeal nerve (thin arrow) on left side.

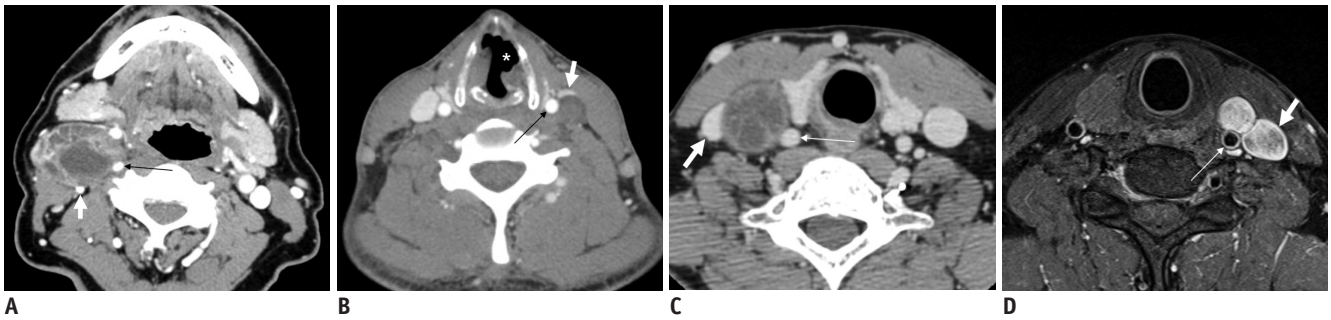

Fig. 16. Axial CT (A-C) and axial contrast-enhanced fat-suppressed T1-weighted (D) images in four different patients with vagal schwannomas (long arrows) demonstrating anatomical variations of vagus nerve within carotid sheath displacing internal jugular vein (short arrows) and internal carotid artery (thin arrow on A) or common carotid artery (thin arrows on B-D) in different directions. Note vocal-cord atrophy (asterisk) caused by vagus nerve palsy on ipsilateral side in **B.**

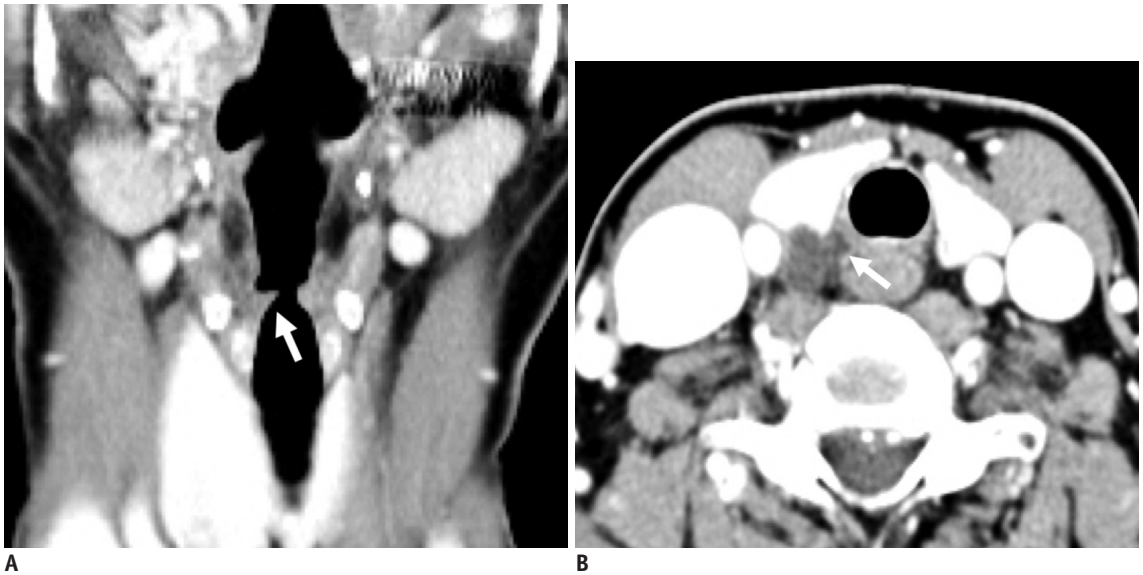

Fig. 17. A 54-year-old male with recent voice change.
A. Reconstructed coronal CT image showing subtle fatty atrophy of right vocal cord (arrow) with secondary dilatation of ipsilateral laryngeal ventricle from vocal cord palsy. **B.** Axial CT image at level of thyroid demonstrating irregular cystic mass insinuating into right tracheoesophageal groove (arrow). Lesion was confirmed as ruptured parathyroid cyst with intracystic bleeding.

Korean Journal of Radiology
KJR

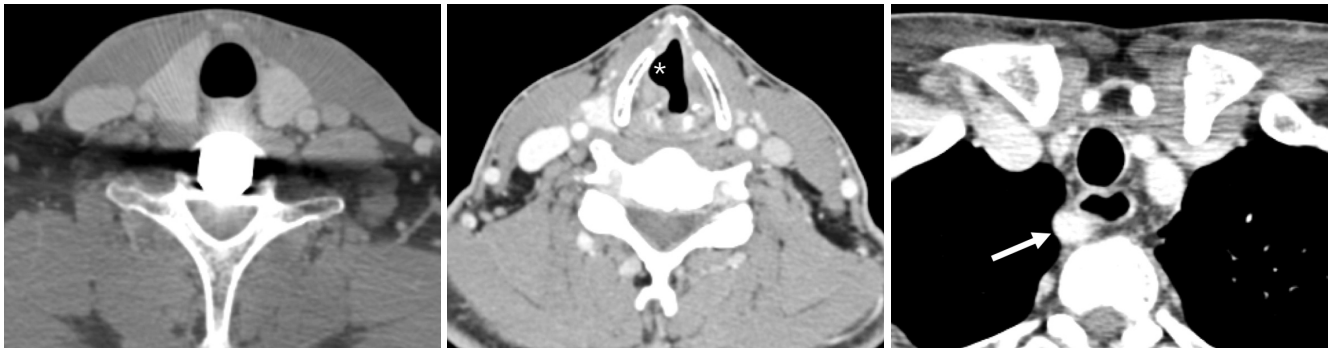

Fig. 18. 55-year-old male with voice change after interbody fusion of C6/7 using anterior approach.
A-C. There is metallic fusion device at C6/7 level **(A)**. Laryngeal ventricle is dilated (asterisk on **B**) due to atrophy of thyroarytenoid muscle on right side. Note aberrant right subclavian artery (arrow on **C**) running posterior to esophagus at thoracic inlet, implying presence of right non-recurrent laryngeal nerve.

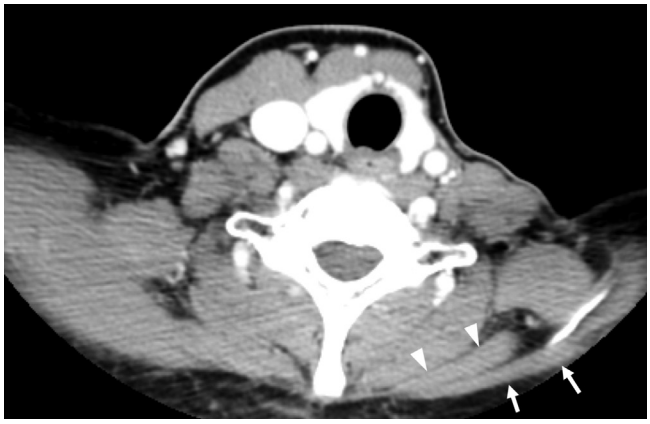

Fig. 19. 32-year-old female who underwent radical neck dissection for advanced tongue cancer. There is neither internal jugular vein nor sternocleidomastoid muscle on left side caused by previous surgery. Note denervation atrophy of left trapezius muscle (arrows) and secondary hypertrophy of rhomboid muscle (arrowheads).

the superior laryngeal artery. The external branch gives rise to motor innervation to the cricothyroid muscle, enabling sound pitch increase by tensing the true vocal cord. The internal branch pierces the thyrohyoid membrane with the superior laryngeal artery and receives sensory fibers from the hypopharynx and supraglottic larynx.

The recurrent laryngeal nerve gives rise to motor innervation to all intrinsic muscles of the larynx except for the cricothyroid muscle as it receives sensory fibers from the larynx below the vocal cord. The nerve loops under the SCA on the right side and the aortic arch on the left side. It then travels upwards in the tracheoesophageal groove posteromedial to both lobes of the thyroid. Both nerves finally enter the larynx by penetrating the thyrohyoid membrane at the level of the cricothyroid joint (Fig. 17).

Non-recurrent laryngeal nerve is a rare anatomical variation with 0.5–0.6% of cases on the right side and 0.04% of cases on the left side (16, 17). A right non-recurrent laryngeal nerve is associated with aberrant right SCA while a left non-recurrent laryngeal nerve is associated with situs inversus. As non-recurrent laryngeal nerve directly goes into the larynx along with the superior or inferior thyroid artery, it is important to recognize the presence of a non-recurrent laryngeal nerve before thyroidectomy or cervical spine surgery using an anterior approach in order to avoid incidental injury to the nerve (Fig. 18) (18, 19).

Spinal Accessory Nerve

The spinal accessory nerve has two components (the cranial root and the spinal root). However, it conveys pure motor innervation to both SCM and the trapezius muscle in the neck as the cranial root separates from the spinal root immediately after exiting the jugular foramen anteromedial to the IJV via the pars vascularis and joins the vagus nerve superior to the inferior vagal ganglion (Fig. 14A). The spinal accessory nerve runs posterolaterally to enter the posterior cervical triangle crossing the IJV at the level of the posterior belly of the digastric muscle. Approximately 80% of spinal accessory nerves cross the IJV anteriorly while the remaining 19% of spinal accessory nerves cross the IJV posteriorly (20). The spinal accessory nerve keeps coursing inferiorly and posteriorly into the posterior neck deep into the SCM. It is superficial to the levator scapulae muscle. It terminates in the trapezius muscle (Fig. 14B). It is practically impossible to see the nerve on conventional CT or MRI. However, it can be consistently detected between the trapezius muscle and the levator scapulae muscle by US (21). More than 90% of spinal accessory nerve injuries are of iatrogenic causes such as neck dissection surgery (either intentional or non-intentional) and excisional biopsy of a

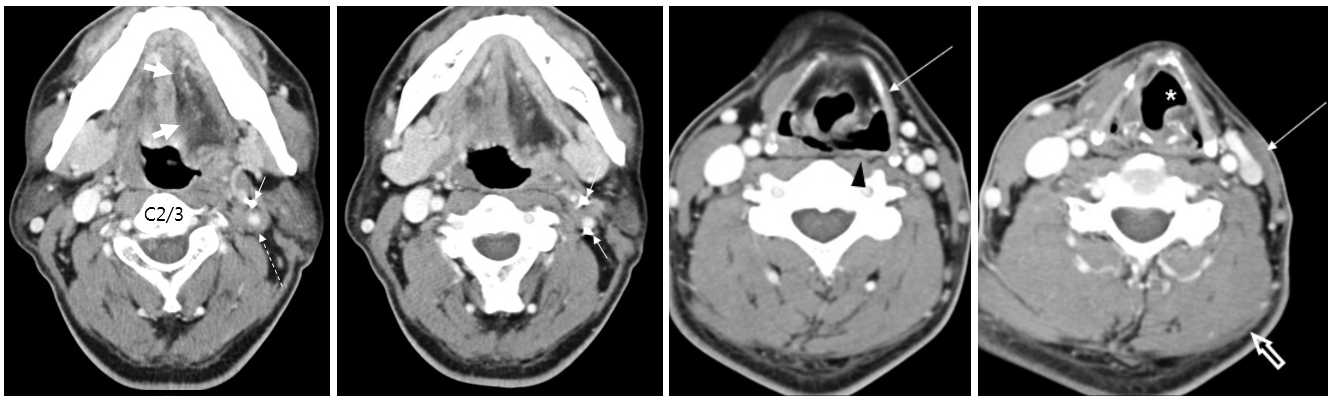

Fig. 20. 47-year-old male with multiple cranial nerve palsy after explosion.
A-D. Axial CT images demonstrating tiny metallic foreign bodies with hematoma (dotted arrow) surrounding left internal carotid artery (short arrows on **A** and **B**). Note that left internal jugular vein is obliterated on **A** and **B**. Left side of tongue (thick arrows on **A**) and left thyrohyoid muscle (long arrow on **C**) are atrophic due to hypoglossal nerve injury. Atrophy of left vocal cord (asterisk on **D**) and left side of hypopharyngeal wall (arrowhead on **C**) suggest vagus nerve injury. Atrophy of left sternocleidomastoid muscle (long arrow on **D**) and left trapezius muscle (empty arrow on **D**) implies damage to spinal accessory nerve.

lymph node due to its close vicinity to cervical lymphatics at cervical levels II, III, and V (Figs. 19, 20) (22, 23).

CONCLUSION

CT and MRI are feasible modalities for evaluating major nerves in the neck and associated pathologic conditions. Knowledge of CT- and MRI-based normal neural anatomy and adjacent relevant landmarks of the neck can avoid complications related to iatrogenic procedures. Understanding the clinical features of nerve damage can assist in the identification of the underlying pathologic process involving neural structures in the neck.

REFERENCES

1. Kiray A, Arman C, Naderi S, Güvencer M, Korman E. Surgical anatomy of the cervical sympathetic trunk. *Clin Anat* 2005;18:179-185
2. Saylam CY, Ozgiray E, Orhan M, Cagli S, Zileli M. Neuroanatomy of cervical sympathetic trunk: a cadaveric study. *Clin Anat* 2009;22:324-330
3. Lee JH, Lee HK, Lee DH, Choi CG, Kim SJ, Suh DC. Neuroimaging strategies for three types of Horner syndrome with emphasis on anatomic location. *AJR Am J Roentgenol* 2007;188:W74-W81
4. Lee JY, Lee JH, Song JS, Song MJ, Hwang SJ, Yoon RG, et al. Superior cervical sympathetic ganglion: normal imaging appearance on 3T-MRI. *Korean J Radiol* 2016;17:e72
5. Hogan QH, Erickson SJ. MR imaging of the stellate ganglion: normal appearance. *AJR Am J Roentgenol* 1992;158:655-659
6. Shin JE, Baek JH, Ha EJ, Choi YJ, Choi WJ, Lee JH. Ultrasound features of middle cervical sympathetic ganglion. *Clin J Pain* 2015;31:909-913
7. Mancall EL, Brock DG. *Cervical plexus*. In: Mancall EL, Brock DG, eds. *Gray's clinical neuroanatomy: the anatomic basis for clinical neuroscience*. Philadelphia: Elsevier Health Sciences, 2011:315-317
8. Bowen BC, Pattany PM, Saraf-Lavi E, Maravilla KR. The brachial plexus: normal anatomy, pathology, and MR imaging. *Neuroimaging Clin N Am* 2004;14:59-85, vii-viii
9. Aralasmak A, Karaali K, Cevikol C, Uysal H, Senol U. MR imaging findings in brachial plexopathy with thoracic outlet syndrome. *AJNR Am J Neuroradiol* 2010;31:410-417
10. van Es HW, Bollen TL, van Heesewijk HP. MRI of the brachial plexus: a pictorial review. *Eur J Radiol* 2010;74:391-402
11. Ha EJ, Lee JH, Lim HK, Bae Kim W, Baek JH. Identification of continuity of transected nerve on sonography after neck dissection: direct sign of traumatic neuroma. *Thyroid* 2011;21:1385-1387
12. Ha EJ, Baek JH, Lee JH, Kim YJ, Kim JK, Kim TY, et al. Characteristic ultrasound feature of traumatic neuromas after neck dissection: direct continuity with the cervical plexus. *Thyroid* 2012;22:820-826
13. Ha EJ, Baek JH, Lee JH, Kim JK, Shong YK. Clinical significance of vagus nerve variation in radiofrequency ablation of thyroid nodules. *Eur Radiol* 2011;21:2151-2157
14. Felten DL, O'Banion MK, Maida ME. *Brain stem and cerebellum*. In: Felten DL, O'Banion MK, Maida ME, eds. *Netter's atlas of neuroscience*. Philadelphia: Elsevier Health Sciences 2015:247-287
15. Park JK, Jeong SY, Lee JH, Lim GC, Chang JW. Variations in the course of the cervical vagus nerve on thyroid ultrasonography. *AJNR Am J Neuroradiol* 2011;32:1178-1181
16. Henry JF, Audiffret J, Denizot A, Plan M. The nonrecurrent inferior laryngeal nerve: review of 33 cases, including two on the left side. *Surgery* 1988;104:977-984

17. Toniato A, Mazzarotto R, Piotto A, Bernante P, Pagetta C, Pelizzo MR. Identification of the nonrecurrent laryngeal nerve during thyroid surgery: 20-year experience. *World J Surg* 2004;28:659-661
18. Chen CC, Huang YC, Lee ST, Chen JF, Wu CT, Tu PH. Long-term result of vocal cord paralysis after anterior cervical disectomy. *Eur Spine J* 2014;23:622-626
19. Jung A, Schramm J. How to reduce recurrent laryngeal nerve palsy in anterior cervical spine surgery: a prospective observational study. *Neurosurgery* 2010;67:10-15; discussion 15
20. Saman M, Etebari P, Pakdaman MN, Urken ML. Anatomic relationship between the spinal accessory nerve and the jugular vein: a cadaveric study. *Surg Radiol Anat* 2011;33:175-179
21. Hong MJ, Baek JH, Kim DY, Ha EJ, Choi WJ, Choi YJ, et al. Spinal accessory nerve: ultrasound findings and correlations with neck lymph node levels. *Ultraschall Med* 2014 Dec 17 [Epub]. http://dx.doi.org/10.1055/s-0034-1385673
22. Kim DH, Cho YJ, Tiel RL, Kline DG. Surgical outcomes of 111 spinal accessory nerve injuries. *Neurosurgery* 2003;53:1106-1112; discussion 1102-1103
23. Cappiello J, Piazza C, Nicolai P. The spinal accessory nerve in head and neck surgery. *Curr Opin Otolaryngol Head Neck Surg* 2007;15:107-111